Solution combustion synthesis of $LiMn_2O_4$ fine powders for lithium ion batteries

Chunyu Zhu [a], Akira Nobuta [a], Genki Saito [a], Isao Nakatsugawa [b], Tomohiro Akiyama [a]*

[a]Center for Advanced Research of Energy & Materials, Hokkaido University, Sapporo 060-8628, Japan

[b]Combustion Synthesis Co., Ltd, Kanbara, Shimizuku, Shizuoka 421-3203, Japan.

*Corresponding author: Tel.: +81-11-706-6842; Fax: +81-11-726-0731.

E-mail address: takiyama@eng.hokudai.ac.jp (Tomohiro Akiyama)

Abstract

In this work, fine powders of spinel-type $LiMn_2O_4$ as cathode materials for lithium ion batteries (LIBs) were produced by a facile solution combustion synthesis using glycine as fuel and metal nitrates as oxidizers. Single phase of $LiMn_2O_4$ products were successfully prepared by SCS with a subsequent calcination treatment at 600 to 1000 ºC. The structure and morphology of the powders were studied in detail by X-ray diffraction, scanning electron microscopy and transmission electron microscopy. The electrochemical properties were characterized by galvanostatic charge-discharge cycling and cyclic voltammetry. The crystallinity, morphology, and size of the products were greatly influenced by the calcination temperature. The sample calcined at 900 ºC had good crystallinity and particle sizes between 500 and 1000 nm. It showed the best performance with an initial discharge capacity of 115.6 mAh g^{-1} and a capacity retention of 93% after 50 cycles at a 1 C rate. In comparison, the $LiMn_2O_4$ sample prepared by the solid-state reaction showed a lower capacity of around 80 mAh g^{-1}.

Keywords: combustion synthesis, lithium ion battery, $LiMn_2O_4$, cathode material

1. Introduction

Rechargeable lithium ion batteries have drawn extensive attention as the most promising candidates to power the next generation of electric vehicles because of their excellent properties such as high energy density and light weight [1, 2]. Currently, lithium cobalt oxide ($LiCoO_2$), which is known for its high energy density and good cycling stability, is the most commercialized cathode material for LIBs. However, the high cost and toxicity of cobalt have prevented its use in next-generation green LIBs [3, 4]. Spinel lithium manganese oxide ($LiMn_2O_4$) is an inexpensive and eco-friendly alternative cathode material that can substitute $LiCoO_2$ in high-power lithium ion batteries [5-7]. However, the application of $LiMn_2O_4$ has restricted by several problems such as capacity loss upon long-term cycling and the absence of a scalable production method that generates fine particles.

Conventionally, $LiMn_2O_4$ is prepared by the solid-state reaction (SSR) of lithium and manganese salts. However, the drawbacks of this method, such as long calcination time; slow reaction kinetics, which hinders the formation of pure single-phase product; and lack of control over the particle size have constrained its practical application. To overcome these drawbacks, numerous wet-chemical methods are being used, which include co-precipitation [8-10], hydrothermal synthesis [11, 12], the sol-gel based solution combustion synthesis [13-15], and spray drying method [7, 16-19]. Among these, solution combustion synthesis (SCS) is a promising method, which is based on a highly exothermic, self-sustaining reaction generated by heating a solution mixture of aqueous metal salts and fuels such as urea, citric acid, and glycine. It has been used to synthesize a variety of compounds, including binary and complex oxides such as ferrites, spinels, and perovskites. It not only yields nanosized particles exhibiting large specific surface areas but also enables uniform (homogeneous) doping of trace amounts of various elements in a single step [20, 21].

In this paper, we describe the glycine-nitrate based combustion synthesis of $LiMn_2O_4$ fine particles and their electrochemical characterization for use as the cathode material in lithium-ion batteries.

2. Experimental

Material preparation: All reagents used in this study were commercially available and used as supplied without further purification: lithium nitrate ($LiNO_3$, 99.9%, Kishida Chemical Co., Ltd., Japan), manganese nitrate ($Mn(NO_3)_2$, 50% w/w aqueous solution, Alfa Aesar), glycine (H_2NCH_2COOH, > 99%, Kishida Chemical Co., Ltd., Japan), manganese oxide (MnO, 99%, High Purity Chemicals), lithium carbonate (Li_2CO_3, 99.99%, High Purity Chemicals).

Figure 1 shows the schematic diagram of the SCS of the $LiMn_2O_4$ precursor. In a typical synthesis required for preparing 3 g of $LiMn_2O_4$, lithium nitrate and manganese nitrate were taken in a molar ratio of Li:Mn = 1.1:2 (10% excess of Li) and dissolved in excess distilled water in an alumina crucible. The homogenous solutions were subsequently mixed with glycine fuel (so as to make the molar ratio of glycine to nitrates = 1) and magnetically stirred. The as-prepared solutions containing metal nitrates and glycine were heated on a hot plate while stirring to evaporate excess water until gels were formed. The as-prepared sol-gel in the crucible was transferred to a lab-made combustion synthesis apparatus, as shown in Figure 1. The reactor consisted of a stainless-steel bin with a long vertical stainless-steel mesh chimney, which enabled the safe removal of large amounts of gases during combustion, leaving behind the ash reactant remnants in the reactor to be collected after the reaction. The reactor was placed on a heater, which was pre-heated to and maintained at 400 ºC. The viscous sol-gel mixtures self-ignited under heating and produced voluminous ashes along large amounts of gases. To obtain $LiMn_2O_4$, the SCSed precursor was subsequently calcined between 600 and 1000 ºC for 10 h.

For comparison, $LiMn_2O_4$ was also produced by the conventional SSR process. The starting materials were MnO and Li_2CO_3 with the Li source in 10% excess. The starting regeants were ball-milled in a planetary-type pulverizer using zirconium oxide grinding bowl and balls. A powder to ball ratio of 1:4 was used. The powders were milled for 4 h in ethanol at a rotation rate of 300 rpm (rotation per minute). The milled powders were dried at 100 ºC to evaporate ethanol, and calcined at 900 ºC for 10 h to produce $LiMn_2O_4$.

Material characterization: Powder X-ray diffraction (XRD, Rigaku Miniflex, Cu-Kα) was used to characterize the phase compositions of the obtained materials. Scanning electron

microscopy (SEM, JEOL, JSM-7400F) and transmission electron microscopy (TEM, JEM-2010 F) were used for observing the morphology and structure. The decompostion behavior of the SCSed precursor was studied using a combined thermogravimetric and differential scanning calorimetry (TG/DSC) analyzer (Mettler Toledo). Samples were subjected to a heating rate of 10 ^{o}Cmin^{-1} in air atmosphere.

Electrochemical characterization: Electrochemical characterization was carried out in two-electrode Swagelok-type cells as described in our previous study [22]. The working electrode consisted of an active material, conductive carbon (acetylene black), and a polymer binder (polyvinylidene fluoride (PVDF)) in a weight ratio of 80:10:10. The cathode materials in this study were mixed with *N*-methyl-2-pyrrolidone (NMP) to form a slurry. The blended slurries were cast onto an aluminum foil current collector and dried at 110 ^{o}C in a vacuum oven for 12 h. The dried electrodes were punched into 10 mm disks. Metallic lithium disk of 10 mm in diameter was used as the counter and reference electrode. The cell was assembled in an Ar-filled glove-box. A solution of 1 M lithium hexafluorophosphate ($LiPF_6$) in ethylene carbonate (EC)/dimethyl carbonate (DMC) (1:1 in volume) was used as the electrolyte. A celgard polypropylene membrane was used as the separator. The cells were galvanostatically cycled between 3.2 and 4.4 V at a current density of 1 C (a rate of 1 C corresponds to a full charge/discharge of the theoretical capacity in 1 h) versus Li/Li^{+} at room temperature using a battery tester (KIKUSUI, PFX2011). Cyclic voltammetry (CV) measurements were performed using a potentiostat/galvanostat apparatus (Autolab, PGSTAT128N). Scanning was performed over the voltage range of 3.4 to 4.5 V at a rate of 0.1 mVs^{-1}.

3. Results and discussion

3.1 Solution combustion synthesis of $LiMn_2O_4$

Figure 2 shows the TG and DSC curves of the SCSed precursor. A minor weight decrease at lower than 100 ºC is due to the loss of combined water in the precursor, and the slight weight increase at around 160-250 ºC is thought to be caused by the oxidation of the SCSed precursor. The SCSed precursor may contain complex intermediate substances such as oxides and carbonaceous residue etc. A large weight loss at ~250–360 ºC was observed, which could be attributed to the decomposition of the SCSed intermediate products such as the carbonaceous residue. These entail that for the formation of the final product $LiMn_2O_4$, further calcination at temperatures exceeding 360 ºC is needed after the SCS.

Figure 3 shows the XRD patterns of the calcined samples. The pattern of the SCSed precursor is also presented for comparison, which indicates an amorphous product. The peaks of the calcined samples can be indexed to a single-phase of spinel-type $LiMn_2O_4$ with Fd3m space group (JCPDS card No. 35-0782), confirming the successful synthesis of the compound by SCS with subsequent calcination. The peaks of the calcined samples became sharper with an increase in the calcination temperature, indicating that the samples obtained at higher temperatures have better crystallinity. The crystallite size, *t*, of these samples was calculated using Scherer's equation:

$$t = \frac{K\lambda}{B\cos\theta} \qquad (1)$$

where K is the shape factor (K = 0.9 in study), λ is the X-ray wavelength, B is the line broadening (measured in radians) at half the maximum intensity, and θ is the Bragg angle. The most intense peak at 2θ = 18.7º was used for the calculation. Each sample was scanned three times to obtain an average value. The crystallite sizes calculated were 17.4 nm, 29.4 nm, 46.6 nm, 52.0 nm, and 53.0 nm for the samples calcined at 600 ºC, 700 ºC, 800 ºC, 900 ºC, and 1000 ºC, respectively. The correlation between the crystallite size and the calcination temperature is plotted in Figure 4.

Figure 5 shows the SEM images of the SCSed precursor and the samples calcined at

different temperatures. The SCSed precursor consisted of porous particles because of the emission of a large amount of gases during combustion. After the precursor was calcined at 600 and 700 ºC, the grains of the porous particles appear to have grown larger. With an increase in the calcination temperature, the relatively small grains of the porous particles grew larger to about 300–800 nm at 800 ºC and to 500–1000 nm at 900 ºC, which were also agglomerated. When the calcination temperature was as high as 1000 ºC, the samples showed large particles of about 1–6 μm in size, which could be due to severe sintering effect. Figure 6 shows the TEM images and selected area diffraction pattern of the sample calcined at 900 ºC. Sintered particles with diameters of less than 1 μm can be clearly seen.

Since the electrochemical properties of cathode materials are significantly influenced by their crystallinity and particle size, calcination temperature becomes an important parameter for obtaining the best product. For example, it is commonly observed that particles with high crystallinity give better electrochemical performance, but, particles with a smaller size and a higher surface area may show good electrochemical properties because of better mass-electrolyte contact and shortened Li^+ ion and electron diffusion routes. For calcined samples, a low calcination temperature may lead to small particles having low crystallinity, whereas a high calcination temperature will lead to the opposite effect. Therefore, to get the right combination of crystallinity and particle size toward a particular electrochemical performance, the calcination temperature must be optimized.

3.2 Electrochemical properties

Figure 7 shows the cycling performance and the first cycle of discharge curves for the samples calcined at different temperatures. As can be seen from the discharge profiles (charge profiles show similar curves in the opposite direction), the samples exhibit two plateaus at around 3.9 and 4.1 V, indicating the two-step oxidation/reduction reaction for the spinel $LiMn_2O_4$, which also corresponds to the redox peaks in the CV curves, as discussed in the following section. The initial discharge capacities were 83.7, 96.3, 106.9, 115.6, and 98.2 $mAhg^{-1}$ at the rate of 1 C for the samples calcined at 600, 700, 800, 900, and 1000 ºC, respectively. The discharge capacities after 50 cycles for these samples were 84.1, 95.9, 94.0, 107.5, and 82.6 mAh g^{-1}, respectively. Clearly, the sample calcined at 900 ºC showed the

highest capacity during the 50 cycles of charge-discharge, and the retention efficiency was 93% after 50 cycles. The optimized SCSed sample showed better cycling performance than some reported $LiMn_2O_4$ prepared by sol-gel methods. For example, the multi-faceted $LiMn_2O_4$ cathode material, which was produced by a carbon exo-templating sol-gel combustion process [13], delivered an initial discharge capacity of only 110 mA h g^{-1} at a current density of 0.05 mA cm^{-2} and degraded very quickly. The citrate-based combustion synthesized $LiMn_2O_4$ [15] showed an excellent initial specific capacity of 130 mAh g^{-1} but the specific capacity dropped to 107 mAh g^{-1} after only 20 cycles at a current density of 0.26 mA cm^{-2}.

CV tests were employed to analyze the oxidation/reduction and phase transformation processes during the reactions at the electrode. Figure 8-(a) shows the first three cycles of the cell made with the cathode sample calcined at 900 ºC. The CVs show a slight shift of the oxidation and reduction peaks and reduced peak area upon cycling, indicating a change in the surface structure and composition of the spinel electrode and a minor decrease in the discharge capacity, as confirmed by the charge-discharge cycling test discussed above.[23] Figure 8-(b) provides the comparison between the initial CVs of the samples calcined at different temperatures. The CV curves exhibit a couple of distinct redox peaks, which indicate the two-stage Li^+ extraction/insertion from/into the spinel phase and are consistent with the two-plateaus detected in the charge/discharge profiles discussed above. The sample calcined at 900 ºC exhibits the highest peak current and peak area, which indicates higher discharge capacity than the other samples. The samples produced at lower temperatures (or at 1000 ºC) exhibit weaker peaks and smaller peak areas, and the two redox peaks are also less distinguishable, which indicates poorer electrode reactivity as compared to that of the sample calcined at 900 ºC. These observations by CV are commensurate with the charge-discharge cycling results.

$LiMn_2O_4$ was also produced by the conventional SSR process by calcining the milled mixture of MnO and Li_2CO_3 at 900 ºC for 10 h. Figure 9-(a) shows the XRD patterns of the SSRed sample in comparison to those of the SCSed sample. Both patterns indicate a single phase of spinel-type $LiMn_2O_4$. However, the charge-discharge cycling performance indicated a lower capacity of around 80 mAh g^{-1} for the SSRed sample as compared to that for the

SCSed sample (115.6 mAh g^{-1}; see Figure 9-(b)). The SSRed sample showed a large particle size of around 1–10 μm as confirmed by the SEM observation, which was similar to the SCSed sample calcined at 1000 ºC.

4. Conclusions

Single phase spinel-type $LiMn_2O_4$ powders were successfully produced by a glycine-nitrate combustion synthesis process, followed by calcination at 600 to 1000 ºC. The crystallinity, particle morphology, and particle size were greatly influenced by the calcination temperature, which correspondingly affected the electrochemical performance. Electrochemical characterization by galvanostatic charge-discharge cycling and CV indicated that the SCS sample calcined at 900 ºC showed the best performance with an initial discharge capacity of 115.6 mAh g^{-1} and a capacity retention of 93% after 50 cycles at a 1 C rate. However, in comparison, the $LiMn_2O_4$ sample prepared by the conventional SSR showed a lower capacity of around 80 mAh g^{-1}. The results here indicate that the glycine-nitrate SCS process is an attractive method for the fabrication of cost-effective fine cathode powders for lithium secondary batteries.

References

[1] B. Scrosati, J. Garche, Lithium batteries: Status, prospects and future, Journal of Power Sources, 195 (2010) 2419-2430.

[2] V. Etacheri, R. Marom, R. Elazari, G. Salitra, D. Aurbach, Challenges in the development of advanced Li-ion batteries: a review, Energy & Environmental Science, 4 (2011) 3243-3262.

[3] B. Xu, D. Qian, Z. Wang, Y.S. Meng, Recent progress in cathode materials research for advanced lithium ion batteries, Materials Science and Engineering: R: Reports, 73 (2012) 51-65.

[4] H.-E. Wang, D. Qian, Z.-g. Lu, Y.-k. Li, Synthesis and electrochemical properties of $LiMn_2O_4$ and $LiCoO_2$-coated $LiMn_2O_4$ cathode materials, Journal of Alloys and Compounds, 517 (2012) 186-191.

[5] C. Wan, M. Wu, D. Wu, Synthesis of spherical $LiMn_2O_4$ cathode material by dynamic sintering of spray-dried precursors, Powder Technology, 199 (2010) 154-158.

[6] K. Kanamura, H. Naito, T. Yao, Z.-i. Takehara, Structural change of the $LiMn_2O_4$ spinel structure induced by extraction of lithium, Journal of Materials Chemistry, 6 (1996) 33-36.

[7] I. Taniguchi, N. Fukuda, M. Konarova, Synthesis of spherical $LiMn_2O_4$ microparticles by a combination of spray pyrolysis and drying method, Powder Technology, 181 (2008) 228-236.

[8] H.W. Chan, J.G. Duh, S.R. Sheen, $LiMn_2O_4$ cathode doped with excess lithium and synthesized by co-precipitation for Li-ion batteries, Journal of Power Sources, 115 (2003) 110-118.

[9] A.R. Naghash, J.Y. Lee, Preparation of spinel lithium manganese oxide by aqueous co-precipitation, Journal of Power Sources, 85 (2000) 284-293.

[10] R. Thirunakaran, R. Ravikumar, S. Gopukumar, A. Sivashanmugam, Electrochemical evaluation of dual-doped $LiMn_2O_4$ spinels synthesized via co-precipitation method as cathode material for lithium rechargeable batteries, Journal of Alloys and Compounds, 556 (2013) 266-273.

[11] K. Kanamura, K. Dokko, T. Kaizawa, Synthesis of Spinel $LiMn_2O_4$ by a Hydrothermal Process in Supercritical Water with Heat-Treatment, Journal of the Electrochemical Society, 152 (2005) A391-A395.

[12] C.H. Jiang, S.X. Dou, H.K. Liu, M. Ichihara, H.S. Zhou, Synthesis of spinel $LiMn_2O_4$ nanoparticles through one-step hydrothermal reaction, Journal of Power Sources, 172 (2007) 410-415.

[13] M.W. Raja, S. Mahanty, R.N. Basu, Multi-faceted highly crystalline $LiMn_2O_4$ and $LiNi_{0.5}Mn_{1.5}O_4$ cathodes synthesized by a novel carbon exo-templating method, Solid State Ionics, 180 (2009) 1261-1266.

[14] B.J. Hwang, R. Santhanam, D.G. Liu, Characterization of nanoparticles of $LiMn_2O_4$ synthesized by citric acid sol–gel method, Journal of Power Sources, 97–98 (2001) 443-446.

[15] K. Du, H. Zhang, Preparation and performance of spinel $LiMn_2O_4$ by a citrate route with combustion, Journal of Alloys and Compounds, 352 (2003) 250-254.

[16] S. Hirose, T. Kodera, T. Ogihara, Synthesis and electrochemical properties of Li-rich spinel type $LiMn_2O_4$ powders by spray pyrolysis using aqueous solution of manganese carbonate, Journal of Alloys and Compounds, 506 (2010) 883-887.

[17] C. Wan, M. Cheng, D. Wu, Synthesis of spherical spinel $LiMn_2O_4$ with commercial manganese carbonate, Powder Technology, 210 (2011) 47-51.

[18] T. Ogihara, H. Aikiyo, N. Ogata, K. Katayama, Y. Azuma, H. Okabe, T. Okawa, Particle morphology and battery properties of lithium manganate synthesized by ultrasonic spray pyrolysis, Advanced Powder Technology, 13 (2002) 437-445.

[19] K. Myojin, T. Ogihara, N. Ogata, N. Aoyagi, H. Aikiyo, T. Ookawa, S. Omura, M. Yanagimoto, M. Uede, T. Oohara, Synthesis of non-stoichiometric lithium manganate fine powders by internal

combustion-type spray pyrolysis using gas burner, Advanced Powder Technology, 15 (2004) 397-403.
[20] A. Mukasyan, P. Dinka, Novel approaches to solution-combustion synthesis of nanomaterials, International Journal of Self-Propagating High-Temperature Synthesis, 16 (2007) 23-35.
[21] S.T. Aruna, A.S. Mukasyan, Combustion synthesis and nanomaterials, Current Opinion in Solid State and Materials Science, 12 (2008) 44-50.
[22] C. Zhu, G. Saito, T. Akiyama, A new $CaCO_3$-template method to synthesize nanoporous manganese oxide hollow structures and their transformation to high-performance $LiMn_2O_4$ cathodes for lithium-ion batteries, Journal of Materials Chemistry A, DOI: 10.1039/C3TA11066D (2013).
[23] M.V. Reddy, S.S. Manoharan, J. John, B. Singh, G.V. Subba Rao, B.V.R. Chowdari, Synthesis, Characterization, and Electrochemical Cycling Behavior of the Ru-Doped Spinel, $Li[Mn_{2-x}Ru_x]O_4$ ($x = 0$, 0.1, and 0.25), Journal of the Electrochemical Society, 156 (2009) A652-A660.

Figure 1. Schematic diagram of the experimental setup used for solution combustion synthesis.

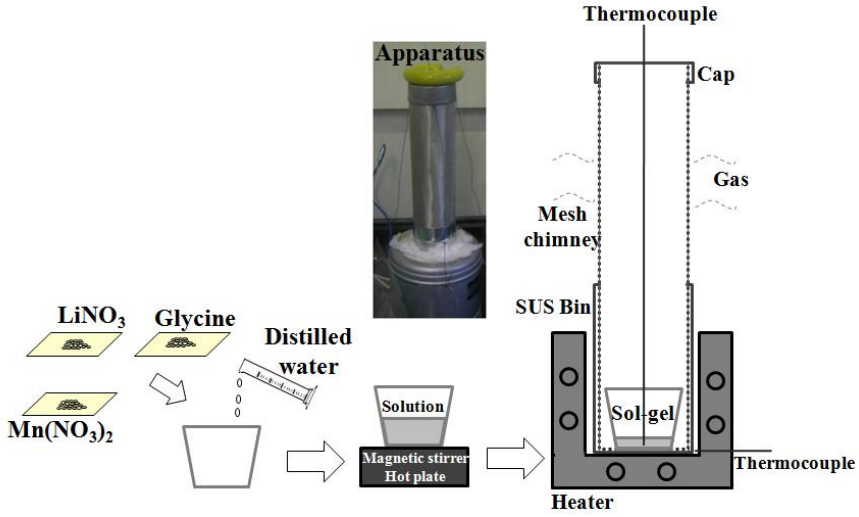

Figure 2. TG and DSC curves of the SCSed precursor obtained under air atmosphere at a heating rate of 10 ^{o}Cmin^{-1}.

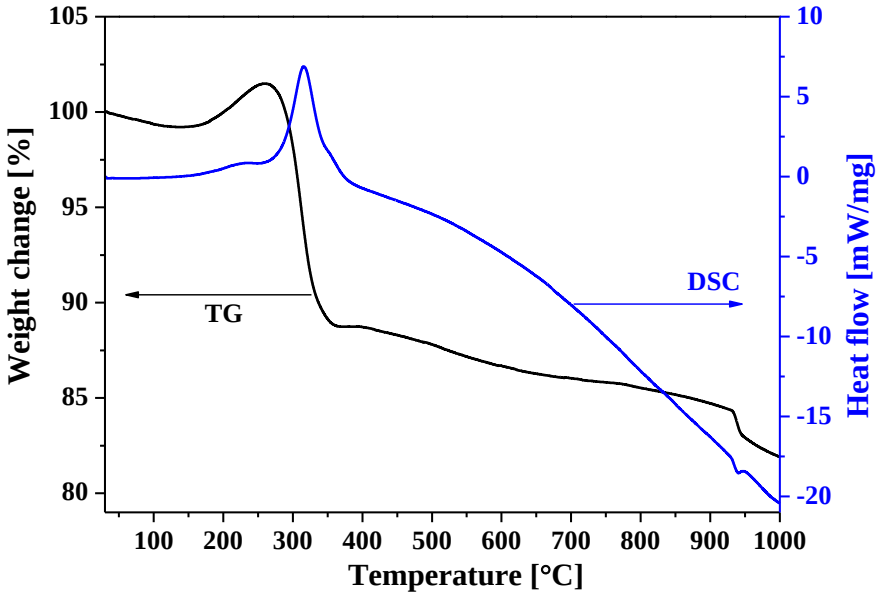

Figure 3. XRD patterns of the samples calcined at different temperatures in comparison to those of the SCSed precursor.

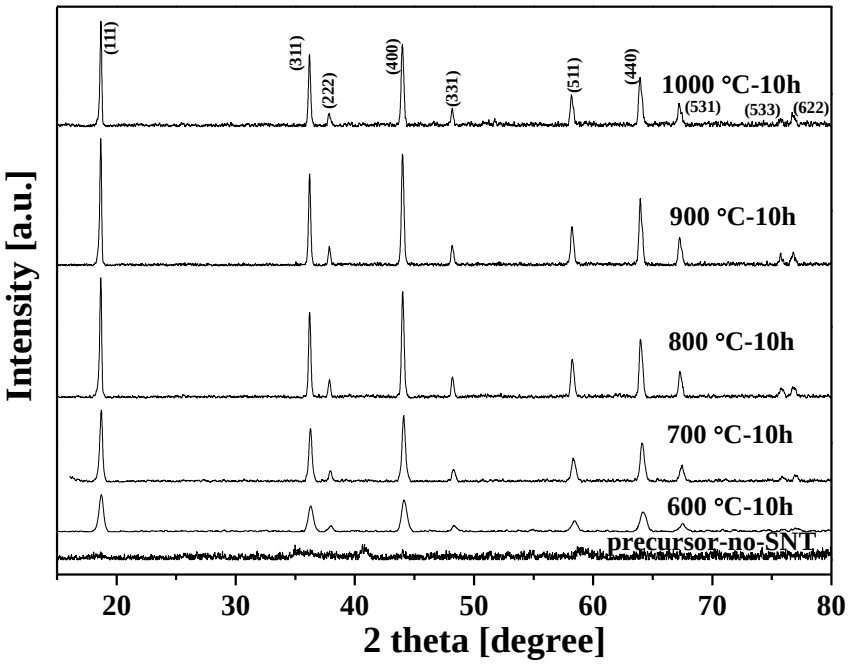

Figure 4. Crystallite sizes (calculated by Scherrer's equation) of the SCSed samples calcined at different temperatures.

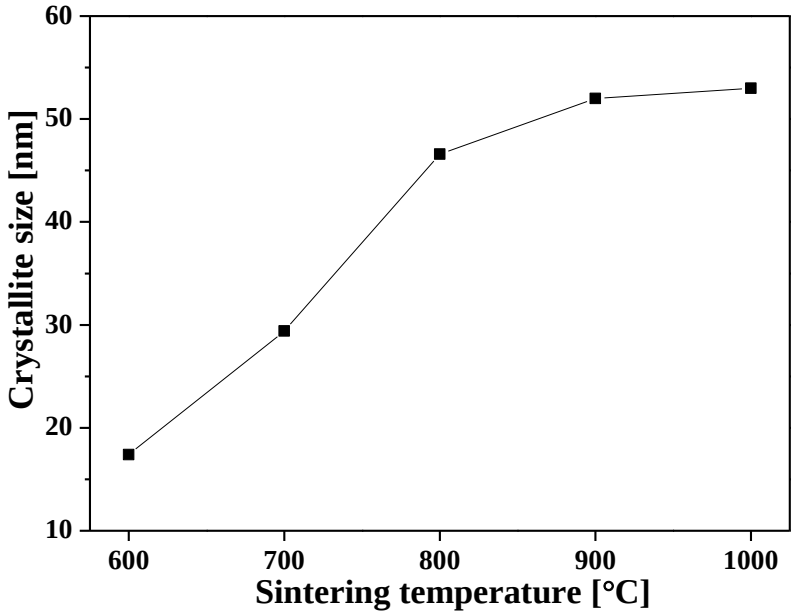

Figure 5. SEM images of the SCSed precursor and calcined samples. Insets show the samples at higher magnification.

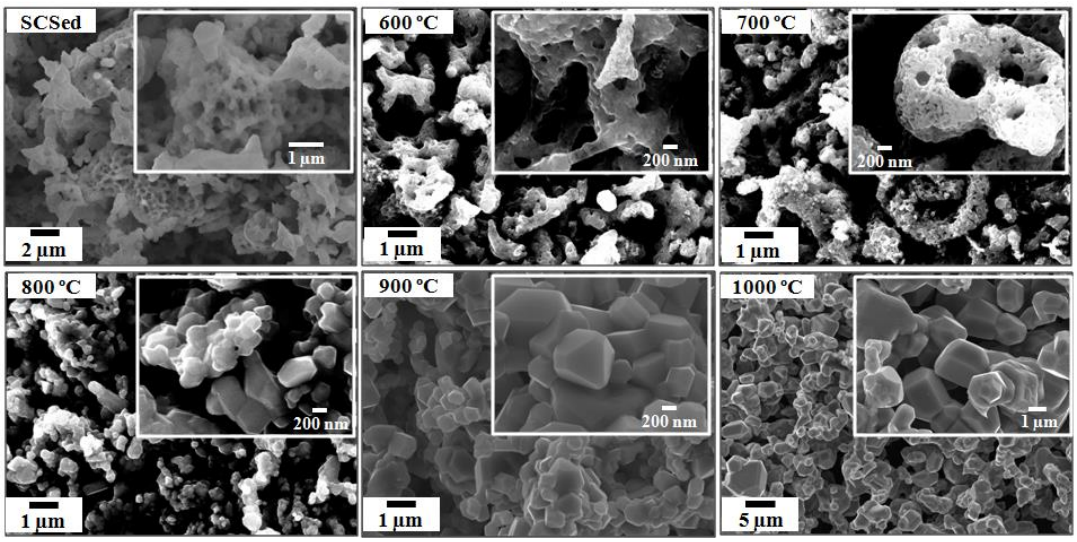

Figure 6. Typical TEM images and selected area diffraction pattern of the calcined sample at 900 °C.

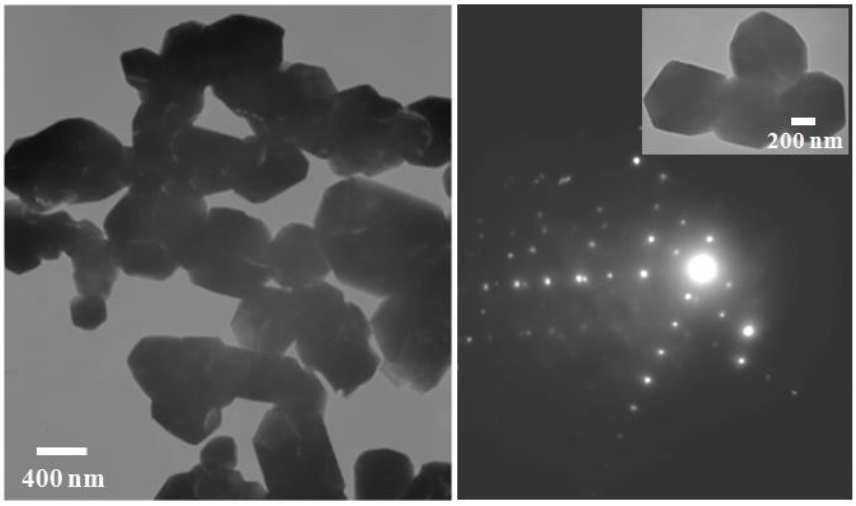

Figure 7. (a) Cycling performance and (b) initial discharge curves of the samples calcined at different temperatures.

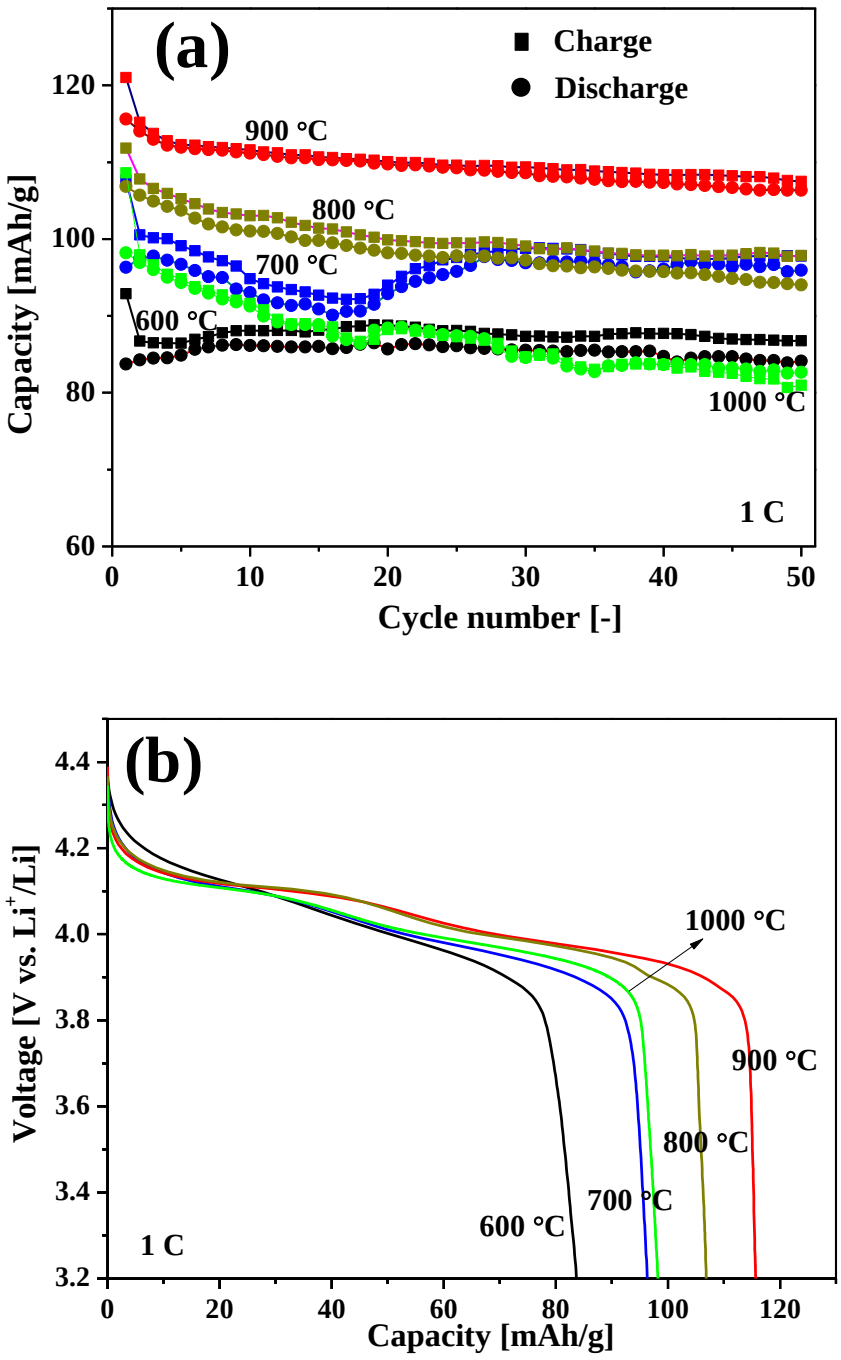

Figure 8. CV curves of the electrodes made with $LiMn_2O_4$. (a) The initial three cycles of the CV curves of the sample calcined at 900 ºC. (b) The first cycle of CV curves of the $LiMn_2O_4$ samples calcined at different temperatures. The scan rate was 0.1 mVs^{-1}.

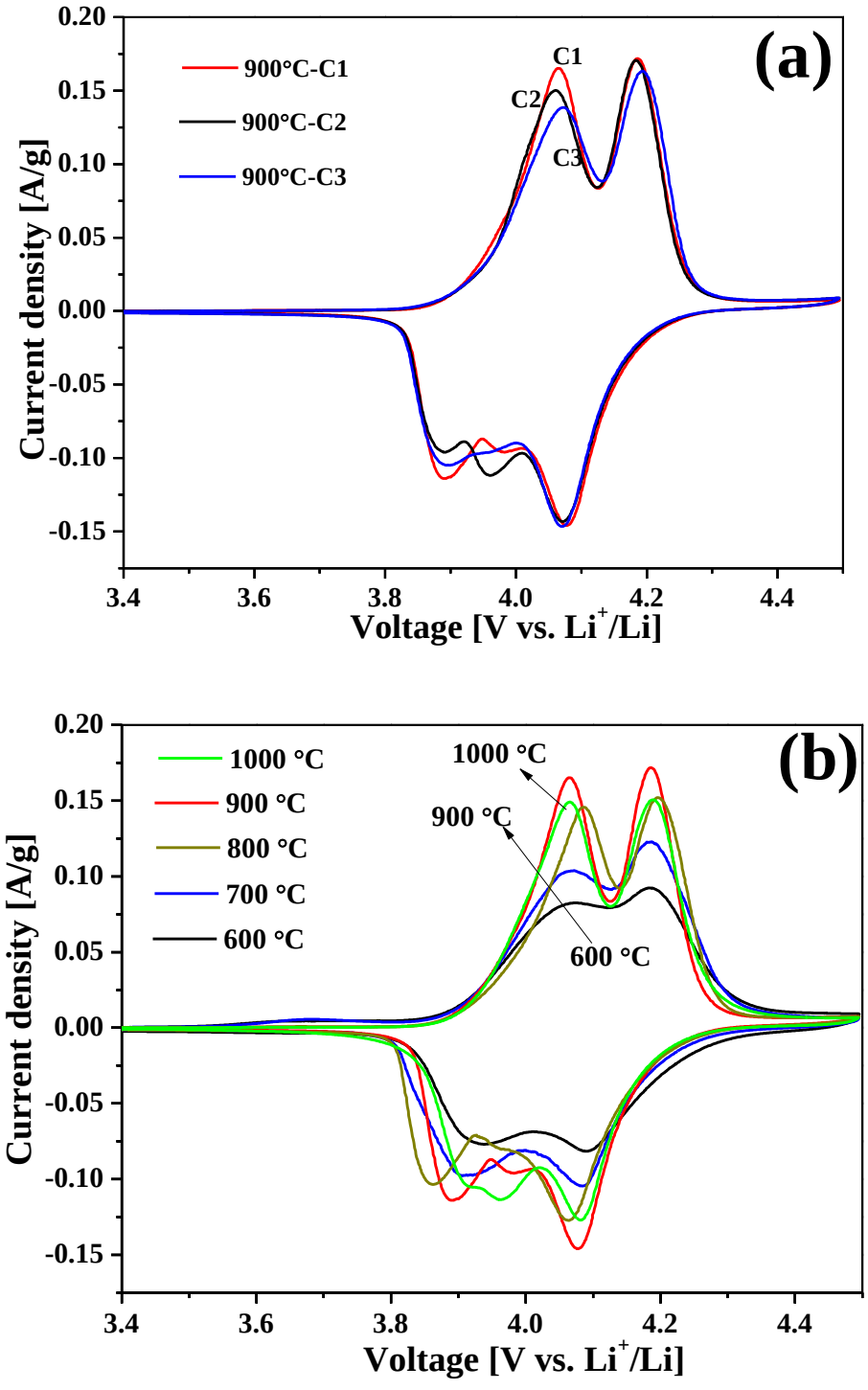

Figure 9. XRD patterns and cycling performance of the SSRed $LiMn_2O_4$, in comparison to those of the SCSed sample. Inset shows the SEM image of the SSRed sample.